

## UC Merced

### UC Merced Previously Published Works

#### Title

Collaboratively Adaptive Vibration Sensing System for High-fidelity Monitoring of Structural Responses Induced by Pedestrians

#### Permalink

<https://escholarship.org/uc/item/4dw306tx>

#### Authors

Pan, Shijia  
Xu, Susu  
Mirshekari, Mostafa  
[et al.](#)

#### Publication Date

2023-06-03

#### DOI

10.3389/fbuil.2017.00028

Peer reviewed

# Collaboratively Adaptive Vibration Sensing System for High Fidelity Monitoring of Structural Responses Induced by Pedestrians

Shijia Pan<sup>a</sup>, Susu Xu<sup>b</sup>, Mostafa Mirshekari<sup>b</sup>, Pei Zhang<sup>a</sup>, Hae Young Noh<sup>b</sup>

<sup>a</sup>*Electrical and Computer Engineering, Carnegie Mellon University*

<sup>b</sup>*Civil and Environment Engineering, Carnegie Mellon University*

---

## Abstract

This paper presents a collaboratively adaptive vibration monitoring system that captures high fidelity structural vibration signals induced by pedestrians. These signals can be used for various human activity monitoring by inferring information about the impact sources, such as pedestrian footsteps, door open closing, dragging objects. Such applications often require high fidelity (high resolution and low distortion) signals. Traditionally, expensive high resolution and high dynamic range sensors are adopted to ensure sufficient resolution. However, for sensing systems that use low-cost sensing devices, the resolution and dynamic range are often limited; hence this type of sensing methods is not well explored ubiquitously. We propose a low-cost sensing system that utilizes 1) a heuristic model of the investigating excitations and 2) shared information through networked devices to adapt hardware configurations and obtain high fidelity structural vibration signals. To further explain the system, we use indoor pedestrian footstep sensing through ambient structural vibration as an example to demonstrate the system performance. We evaluate the application with three metrics that measure the signal quality from different aspects: the sufficient resolution rate to present signal resolution improvement without clipping, the clipping rate to measure the distortion of the footstep signal, and the signal magnitude to quantify the detailed resolution of the detected footstep signal. In experiments conducted in a school building, our system demonstrated up to 2X increase on the sufficient resolution rate and 2X less error rate when used to locate the pedestrians as they walk along the hallway, compared to a fixed sensing setting.

*Keywords:* Structural vibration sensing, indirect sensing, pedestrian monitoring

---

## 1. Introduction

Structural vibration sensing for pedestrian monitoring has been applied for various spatio-temporal information acquisition purposes. Works have been done on human information monitoring through vibration induced by their activities, including identity [1, 2, 3],

---

*Email addresses:* [shijiapa@cmu.edu](mailto:shijiapa@cmu.edu) (Shijia Pan), [susux@cmu.edu](mailto:susux@cmu.edu) (Susu Xu), [mmirshekari@cmu.edu](mailto:mmirshekari@cmu.edu) (Mostafa Mirshekari), [peizhang@cmu.edu](mailto:peizhang@cmu.edu) (Pei Zhang), [noh@cmu.edu](mailto:noh@cmu.edu) (Hae Young Noh)

*URL:* <https://users.ece.cmu.edu/~shijiapa/> (Shijia Pan)

*Preprint submitted to Frontiers in Built Environment: Structural Sensing*

*November 26, 2019*

12 gender [4, 5], location [6, 7, 8, 9], trajectory [10, 11], traffic [12, 13], activity [14], etc. The  
13 non-intrusive nature of this sensing system makes it a promising ubiquitous sensing method.  
14 Like other sensing systems, structural vibration sensing generally requires three steps in  
15 order to fulfill its purposes: signal acquisition, feature extraction, and information learning.

16 A large amount of research has been focusing on feature extraction and information  
17 learning for different vibration based applications [3, 4, 6, 9, 10, 13]. However, if the raw  
18 signals acquired are already distorted (signal clipping) or of low resolution, the learning can  
19 hardly compensate for such information loss. One way to improve the signal fidelity is to use  
20 sensors with high dynamic range and high resolution. These sensors are often expensive and  
21 impractical for large-scale deployment. On the other hand, our target signals induced by  
22 pedestrian vary in signal strength (amplitude) fast and significantly, hence existing adaptive  
23 hardware settings methods can hardly adapt fast enough to such changes.

24 Therefore, in this paper, we present a low-cost high-fidelity vibration signal acquisition  
25 system targeting at pedestrian induced structural vibration responses. Our system ensures  
26 high signal fidelity by predicting the pedestrian induced vibration signal strength and calcu-  
27 lating the hardware configuration setting required. The predictions mainly are through two  
28 solutions: 1) for each sensor, it applies heuristic models of structural responses and adapts  
29 amplification settings dynamically to maximize signal resolution while minimizing clipping  
30 rate; and 2) for the networked sensors, the system models the structural variation through  
31 multiple locations to improve dynamic adaption of each local amplification setting. Finally,  
32 the system detects and outputs high fidelity pedestrian induced vibrations. In general, our  
33 paper provides the following contributions:

- 34 • We present a hardware system with low-cost off-the-shelf vibration sensors that adapts  
35 hardware configuration (e.g., amplification gains) to obtain high fidelity structural  
36 vibration responses induced by pedestrians.
- 37 • We propose a prediction method that employs both a heuristic model to adapt hard-  
38 ware based on local signal change and a collaborative model to adapt hardware based  
39 on global variance.
- 40 • We apply the system to an application: pedestrian monitoring by footstep induced  
41 vibration and evaluate the system performance in this application.

42 To the best of our knowledge, this is the first work that investigates sensing signal quality  
43 for structural vibration monitoring.

44 The rest of the paper is organized as follows: In Section 2, we detail related work done  
45 on improving signal fidelity and what is the research gap between prior works and this work.  
46 Then, Section 3 presents the overview of the system. Next, in Section 4 and Section 5 , we  
47 introduced the optimization solution for hardware configuration, and the algorithm design  
48 for collaborative adaptation of the hardware. Then in Section 6, we present the system  
49 implementation. Section 7 evaluates the system modules and analyzes their abilities to  
50 preserve footstep induced structural vibrations with high fidelity. Then, in Section 8 we  
51 further discuss the system limitation, trade-offs, and usage. Finally, Section 9 presents the  
52 conclusions of this work.

## 2. Related Work

Prior works that focus on improving sensing signal quality mainly fall into three categories: 1) utilizing expensive enhanced sensors [15], 2) post-processing to restore signal shape [16, 17, 18], and 3) adaptive hardware settings to obtain high fidelity signals [19, 20]. The cost of **enhancing** sensing device to achieve high dynamic sensing range as well as high resolution could make large-scale deployment unrealistic. Previous methods for obtaining high-fidelity sensing data mainly fall into two categories: post- and pre-processing. **Post-processing** methods restore unknown or lost data after data collection [16, 17, 18]. These methods are usually used for audio data and evaluated by signal-to-noise ratio (SNR). Janssen et al. proposed an adaptive interpolation method to restore lost data, with the restrictions that the positions of the unknown samples are known [16]. Miura and his group introduced their clipping removal method through recursive vector projection [18]. Kitic et al. approached the problem from another perspective with iterative hard thresholding and evaluated the results using both signal-to-noise ratio and human listening [17]. However, for those feature-oriented applications such as identification [3] or TDoA-based localization [10], restored data is not dependable enough since it introduces signal artifacts.

**Pre-processing** methods utilize signal processing techniques to predict signal clipping and limit distortion of an amplified signal [21]. In addition, Zhang et al. proposed the robust taking pressure control (RPC) algorithm to adjust the system sensing configuration for better signal collection [20]. For pedestrian induced excitation, the rapid change and variation makes it difficult if not impossible to achieve high fidelity with those methods.

## 3. System Overview

The system goal is to capture high fidelity structural vibration signals induced by indoor pedestrians using low-cost low-dynamic-range sensors. It is achieved by maximizing the signal resolution while avoiding signal clipping. Figure 1 shows the relationship between the modules in the system. The vibration signal is obtained by the analog signal acquisition module, which specifies the sensing configuration used. Then the detected impact signals are sent to a collaborative adaptive prediction module where the sensing configuration is decided based on sensing data from the local device as well as from other networked devices.

The rest of the paper introduces the system based on the application of pedestrian monitoring through footstep induced vibration. The causes of variation in detected human footstep strength mainly fall into two categories: human and environmental. Human variation includes two aspects: 1) the personal level as inconsistencies of individual footstep-to-sensor distance within a series of steps (we refer it as a *trace* in the rest of the paper), and 2) the interpersonal level as variations between individuals. Environmental variation occurs when the sensors are placed at different locations, which have different impact response due to structural factors like beams and partitions.

To accommodate these variations, the system, first of all, needs to have a variety of applicable hardware configurations that support the signal variation range (Section 4). Then the system determines the hardware configuration settings to through the collaboratively adaptive algorithm (Section 5).

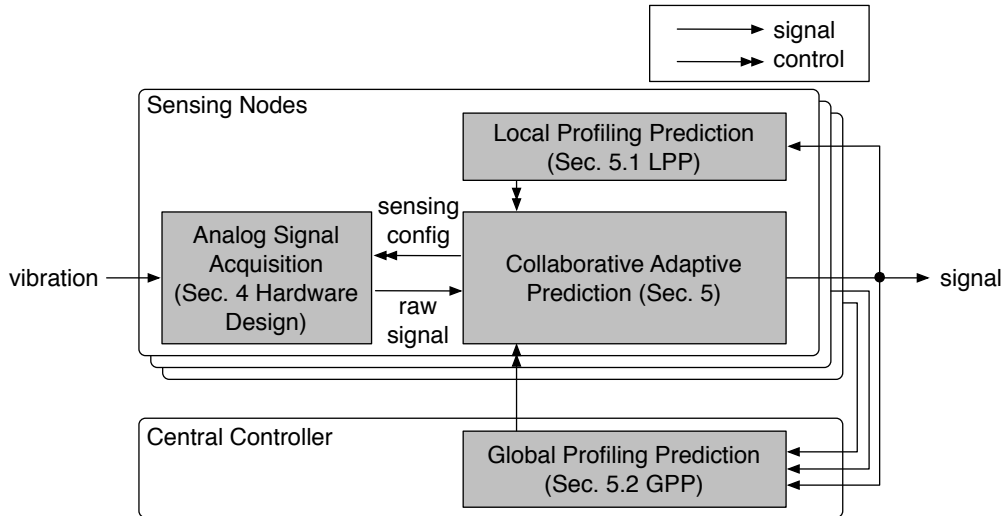


Figure 1: System overview.

#### 94 4. Hardware: Sensing Configuration Optimization

95 The hardware configuration selection is the foundation of the sensing system. The goal  
 96 of the selection is to use minimum number of amplifiers to satisfy the sensing requirement,  
 97 which we solve through an optimization problem. We define an amplified footstep signal  
 98 that is represented by a range of integer values as of ‘sufficient resolution’ when that range  
 99 is over a selected threshold. For a different system or application, this threshold can be  
 100 defined differently. The goal of optimization is to maximize the probability that a detected  
 101 signal falls in the sufficient resolution interval after amplification with a limited number of  
 102 amplifiers. How do we select amplification gain so that amplifiers allow a step signal on a  
 103 surface to have sufficient resolution? First, we explain the relation between the concept of  
 104 amplification and signal resolution (Amplification and Signal Resolution). Next, since the  
 105 optimization mainly targets footstep strength change in a trace due to footstep-to-sensor  
 106 distance variation, we model the distribution of the signal amplitude at different locations on  
 107 a floor plane (Signal Amplitude Distribution). We form the optimization problem (Objective  
 108 Function) to maximize the probability that a signal with the modeled distribution falls in  
 109 the sufficient resolution range with limited amplification settings and obtain the optimal  
 110 solution (Optimal Solution). Finally, the hardware design using the optimal solution is  
 111 discussed.

112 Before we form the optimization problem, we list the notations used in the following  
 113 sections in Table 1. In order to model the amplitude distribution of footstep impulses mea-  
 114 sured by a sensor, we represent the floor with a 2-dimensional X-O-Y Cartesian Coordinate  
 115 plane. Since the calculation depends only on the relative locations of the footsteps and the  
 116 sensor, we simplify the computation by taking the sensor’s location as the origin on the plane  
 117 without losing generality. We make four assumptions to form the optimization problem:

118 **Assumption 1.** *The sensing area  $A$  is a circular area with the sensor at the origin  $(0,0)$ .*

Table 1: Notations

Notation	Descriptions of Notations
$X - O - Y$	Cartesian coordinates of sensor/footstep position
$T$	Input signal amplitude
$T_1$	Output signal threshold 1
$T_2$	Output signal threshold 2
$k$	Signal amplitude measured 1 unit distance from sensor
$d$	Distance between sensor and footstep
$(L_1, L_2)$	Footstep location in X-O-Y
$g_i$	$i$ th amplifier; where $\forall i, 1 < g_i < g_{i+1}$
$n$	Number of amplifiers
$A$	Sensing area
$R$	Radius of A
$F_T(t)$	Cumulative distribution function of T
$F_D(d)$	Cumulative distribution function of d in A

119 **Assumption 2.** Attenuation model  $T \propto \frac{1}{\sqrt{d}}$  [22, 11, 23]. When  $d > R$ , the impulse is  
120 outside the sensing area  $A$ , so we assign  $T = 0$ .

121 **Assumption 3.** The probability distribution of  $(L_1, L_2) \in X-O-Y$  is a uniform distribution,  
122 that is, the probability that a footstep falls on any point in the sensing area is the same.

123 **Assumption 4.** The number of amplifiers is smaller than the least number needed to prop-  
124 erly amplify the raw signal over the whole input signal range  $(\frac{k}{\sqrt{d}}, T_2)$ , i.e., amplification  
125 ranges do not overlap.

Table 2: Amplitude and Resolution

Amplitude	Resolution
$(0, T_1)$	Insufficient
$[T_1, T_2]$	Sufficient
$(T_2, +\infty)$	Clipping (distorted)

126 *4.1. Amplification and Signal Resolution*

127 The analog-to-digital converter using limited number (resolution) of values to describe a  
 128 signal within a specific voltage range; hence, for each impulsive vibration signal investigated,  
 129 the amplification that maximize the resolution is different. For an analog-to-digital converter  
 130 of the specific resolution, a signal that is represented with a large enough number of different  
 131 values is defined as sufficient resolution. This indicates that the amplified signal falls into  
 132 a designated voltage range of  $[T_1, T_2]$ . For different applications requirements, the optimal  
 133 range of  $[T_1, T_2]$  can be different. For example, human identification may require higher  
 134 resolution signal to achieve high accuracy compared to the application of presence detection.  
 135 Thus, identification application may have a higher optimal value for  $T_1$  than that of presence  
 136 detection. We quantify the relation between signal amplitude and resolution level as shown  
 137 in Table 2. If a signal is amplified by the gain of  $g$  and its output falls into the range of  
 138  $[T_1, T_2]$ , then the original range of the signal is  $[\frac{T_1}{g}, \frac{T_2}{g}]$ . In that case, the sufficient resolution  
 139 interval for input signal amplitude is expanded to  $[\frac{T_1}{g}, \frac{T_2}{g}] \cup [T_1, T_2]$ . With multiple available  
 140 amplification gains, say  $1 = g_0 < g_i < g_n$  ( $0 < i < n$ ), the system can cover sufficient  
 141 resolution intervals within the full expected signal range. Although the method is applicable  
 142 for any  $g$  values, considering the footstep signal range, it is practical to assume that the signal  
 143 does not need to be amplified down, therefore we have  $g_0 = 1$  here.

$$SigRange = [\frac{T_1}{g_0}, \frac{T_2}{g_0}] \cup [\frac{T_1}{g_1}, \frac{T_2}{g_1}] \cup \dots \cup [\frac{T_1}{g_n}, \frac{T_2}{g_n}] \quad (1)$$

144 With this definition of *SigRange*, we further interpret the optimization goal as follows.  
 145 Given the number of amplification configurations (amplifier gain)  $n$ , find a set of amplifica-  
 146 tion gains  $1 = g_0 < g_i < g_n$  ( $0 < i < n$ ) so that the probability of the input signal amplitude  
 147 that belongs to the *SigRange* is maximized.

148 *4.2. Signal Amplitude Distribution*

149 To select the optimal amplification setting combination, we need to understand the  
 150 possible signal amplitudes ( $T$ ) and their distribution. To simplify the model, we consider an  
 151 ideal surface described by Assumption 1 and 3 as a start. On an ideal surface, the distance  
 152 ( $d$ ) between the footstep and the sensor affects this distribution. Therefore, we can estimate  
 153 the probability of obtaining a signal of amplitude  $T$  from the probability of a step falling on  
 154 a point of  $d$  away from the sensor, where a relationship between  $d$  and  $T$  as  $T = \frac{k}{\sqrt{d}}$ , ( $k > 0$ )  
 155 can be specified. Based on Assumption 2, the value  $k$  is derived from the absolute value of  
 156 the impulse strength, which is caused by interpersonal level difference and not modeled in  
 157 the optimization problem.

To model the clipping of amplifiers, we define a threshold  $T_2$ : when  $T > T_2$ , the amplitude  
 is too large and exceeds the upper bound output, meaning the signal is clipping. The  
 amplitude in the clipped range  $(T_2, +\infty)$  will always be sensed as the value  $T_2$ . In that case,  
 according to Assumption 2, given the circular area  $A$  around a sensor, we formulate the

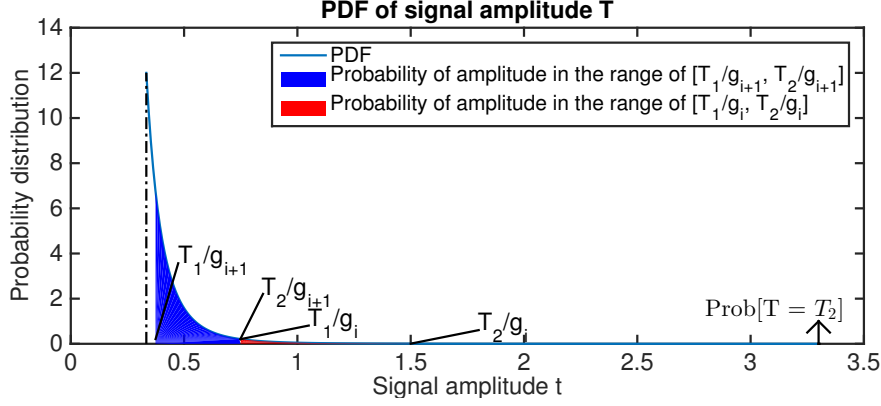


Figure 2: Probability distribution of the signal amplitude  $T$ . Note that the distribution is continuous in interval  $[\frac{k}{\sqrt{R}}, T_2)$  with the function  $f_T(t) = \frac{4k^4}{R^2 t^5}$ , while discrete at  $T = T_2$  due to clipping. This figure shows the scenario where  $k = 1$ ,  $R = 9$  and  $T_2 = 3.3$ . The red region is smaller than the blue region, which means when  $g_i$  increases, the probability that the signal amplitude lies in the sufficient resolution interval also increases. Considering  $d \leq R$ , we can derive that  $\frac{k^2}{T^2} \leq R$ , which leads to  $\forall t \in [\frac{T_1}{g_i}, \frac{T_1}{g_i}], \frac{T_2}{g_i} > \frac{T_1}{g_i} \geq \frac{k}{\sqrt{R}}$ , which is the constraint shown in Eq. 7. In order to prevent overlapping of the red region and the blue region, the constraint in Eq. 8 should be satisfied.

amplitude  $T$  as a function of distance ( $d$ ) and the impulse strength ( $k$ ):

$$T = \begin{cases} T_2 & d \in (0, \frac{k^2}{T_2^2}) \\ \frac{k}{\sqrt{d}} & d \in [\frac{k^2}{T_2^2}, R] \\ 0 & d \in (R, +\infty) \end{cases} \quad (2)$$

Once we understand the relation between  $d$  and  $T$ , in order to derive the distribution of  $T$ , we first calculate the distribution of  $d$ . Assumption 1 defines  $O = (0, 0)$ , so the distance between the sensor and the footstep can be represented as  $d = \sqrt{L_1^2 + L_2^2}$ . Assumption 3 defines the probability distribution of  $(L_1, L_2)$ , which can be applied here to derive the probability distribution of  $d$  as Eq. 3.

$$F_D(d) = \begin{cases} \frac{d^2}{R^2} & 0 \leq d \leq R \\ 1 & d > R \end{cases} \quad (3)$$

Then we can derive the cumulative distribution function (CDF) of the signal amplitude from Eq. 2 and 3, and formulate it in Eq. 4

$$F_T(t) = P(T \leq t) = \begin{cases} 0 & t \in [0, \frac{k}{\sqrt{R}}) \\ 1 - \frac{k^4}{R^2 t^4} & t \in [\frac{k}{\sqrt{R}}, T_2) \\ 1 & t \in [T_2, +\infty) \end{cases} \quad (4)$$



158 Figure 2 indicates that the probability distribution of amplitude is continuous in the  
 159 interval  $[\frac{k}{\sqrt{R}}, T_2)$ , while discrete at  $T = T_2$ . For the continuous part, the probability density  
 160 function of amplitude (PDF)  $f_T(t)$  decreases when  $t$  increases. Together with Assumption  
 161 4, this implies that in the optimal solution, the sufficient resolution intervals of different  
 162 amplifiers should not overlap unless we have more than enough amplifiers to cover the entire  
 163 input signal range, which violates Assumption 4. That is,  $\forall g_i < g_j$ , if  $\frac{T_2}{g_j} > \frac{T_1}{g_i} > \frac{T_1}{g_j}$ , there  
 164 must be  $g'_i < g_i$  and  $\frac{T_2}{g_j} = \frac{T_1}{g'_i}$ , such that probability that amplitude lies in  $[\frac{T_1}{g_j}, \frac{T_2}{g_j}] \cup [\frac{T_1}{g'_i}, \frac{T_2}{g'_i}]$   
 165 is greater than probability that in  $[\frac{T_1}{g_j}, \frac{T_2}{g_j}] \cup [\frac{T_1}{g_i}, \frac{T_2}{g_i}]$  (i.e.,  $F(\frac{T_2}{g_j}) - F(\frac{T_1}{g_j}) < F(\frac{T_2}{g'_i}) - F(\frac{T_1}{g'_i})$ ).

### 166 4.3. Objective Function

167 We use an optimization problem to describe the goal of our amplification setting selection,  
 168 which is to maximize the probability that the vibration signal amplitude lies in the sufficient  
 169 resolution interval. We formulate the optimization problem into Eq. 5.

$$\max_{g_1, \dots, g_n} \sum_{i=0}^n F\left(\frac{T_2}{g_i}\right) - F\left(\frac{T_1}{g_i}\right) \quad (5)$$

$$s.t. \quad 1 < g_i < g_{i+1} \quad \forall i \in \{1, \dots, n-1\} \quad (6)$$

$$\frac{T_1}{g_i} \geq \frac{k}{\sqrt{R}} \quad \forall i \in \{1, \dots, n\} \quad (7)$$

$$\frac{T_2}{g_{i+1}} \leq \frac{T_1}{g_i} \quad \forall i \in \{1, \dots, n-1\} \quad (8)$$

170 Three constraints are applied to the optimization problem:

- 171 1. Constraint in Eq. 5. We simplify the calculation by define the order of amplification  
 172 gain  $g_i$  is monotone increasing with  $i$ . We consider  $g_0$  to represent the scenario where  
 173 there is no amplifier applied, therefore the gain is  $g_0 = 1$ , and  $[\frac{T_1}{g_0}, \frac{T_2}{g_0}]$  is the sufficient  
 174 resolution interval of the raw signal.
- 175 2. Constraint in Eq. 7. Assumption 2 asserts that  $d \leq R$ , which leads to  $\frac{k^2}{T^2} \leq R$ ,  
 176 therefore we can derive that  $\forall t \in [\frac{T_1}{g_i}, \frac{T_2}{g_i}]$ ,  $\frac{T_2}{g_i} > \frac{T_1}{g_i} \geq \frac{k}{\sqrt{R}}$ .
- 177 3. Constraint in Eq. 8. Because  $\forall i, j \in \{1, \dots, n\}$ ,  $(\frac{T_1}{g_i}, \frac{T_2}{g_i})$  can not overlap with  $(\frac{T_1}{g_j}, \frac{T_2}{g_j})$   
 178 and  $g_i < g_{i+1}$ , the signal that gets clipping when  $g_{i+1}$  is used should not be of insuffi-  
 179 cient resolution when the next level of gain  $g_i$  is applied.

### 180 4.4. Optimal Solution

To solve the optimization problem (Section 4.3) using the cumulative distribution func-  
 tion of signal amplitude from Eq. 4, the objective function can be rewritten as

$$S = \frac{k^4}{R^2} \left( \frac{1}{T_1^4} - \frac{1}{T_2^4} \right) \cdot \left( 1 + \sum_{i=1}^n g_i^4 \right) \quad (9)$$

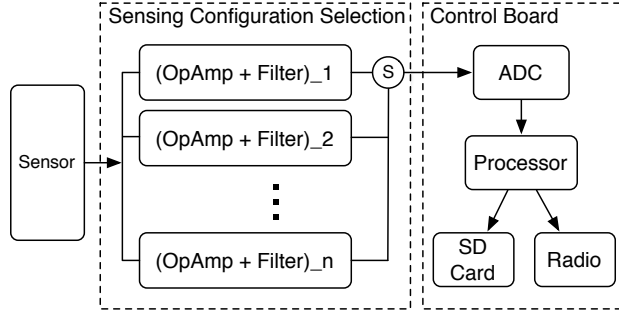


Figure 3: Adaptive amplification module.  $n$  levels of the OpAmp are designed to allow the analog signal to be amplified to different ranges. For each iteration, a level of OpAmp is selected (S), and sent to Analog-to-Digital Converter (ADC). Then the digitized signal is sent to processor for further analysis.

where  $\frac{k^4}{R^2}(\frac{1}{T_1^4} - \frac{1}{T_2^4})$  is a positive constant. Thus, we can maximize the objective function S by maximizing  $\sum_{i=1}^n g_i^4$ , which provides the optimal solution

$$g_i = \left(\frac{T_1}{T_2}\right)^{n-i} \cdot \frac{\sqrt{R} \cdot T_1}{k} \quad \forall i \in \{1, \dots, n\}. \quad (10)$$

181 The variable  $k$  is a structural characteristics determined value affected by the damping factor  
 182 of the structure. This result is used to select the optimal amplification gain values in our  
 183 implementation introduced in Section 4.5.

#### 184 4.5. Hardware Design using Optimal Solution

185 To allow the system to obtain signals with different amplification gains, we design the  
 186 sensing configuration board with multiple amplification settings. As shown in Figure 3, in  
 187 a situation with  $n$  different amplification configurations, the raw signal will go through the  
 188 sensing unit with each one. Instead of collecting signals from all different configurations, the  
 189 system selects the optimal one to obtain the signal. Collecting from  $n$  configurations limits  
 190 the sampling rate to  $1/n$  due to the system sampling rate limitation as well as radio band  
 191 width limitation. Then the signal from the selected configuration is digitized and stored.

192 To obtain the structural variable  $k$  for the model, we generate a modeling impulse (for  
 193 example, a ball-drop with a designated strength) at the edge of the targeting sensing area  
 194 (a designated  $R$  that is determined by the structural noise level), and the system tunes  
 195 amplification gain  $g_n$  to allow the impulse to achieve the highest resolution possible. Then  
 196 we calculate the value  $k$  based on the tuned  $g_n$  and the equation  $g_n = \sqrt{R} \cdot T_1/k$ . After  
 197 that, we calculate the rest of the gain  $g_i$ ,  $i = 0, \dots, n - 1$  based on the defined  $T_1$  and  $T_2$ , as  
 198 well as the structural factor  $k$ .

### 199 5. Algorithm: Collaborative Adaptive Prediction

200 In order to adapt to signal strength variation caused by pedestrian locations and struc-  
 201 tural factors, our system operates on two interconnected levels of feedback control as shown

202 in Figure 1: local profiling prediction and global profiling prediction. Local profile prediction  
 203 refers to the process by which an individual sensing unit uses the data it collects to predict  
 204 the optimal amplification settings for the next footstep-induced signal. Global profile pre-  
 205 diction refers to the collaborative prediction performed by multiple sensing units operating  
 206 with one another. Together, they serve to provide feedback using known signals to infer and  
 207 predict optimal amplification selections for future signals on both local and global levels.

### 208 5.1. Local Profile Prediction (LPP)

209 The goal of the LPP is to achieve high resolution for the low signal-to-noise ratio step  
 210 signals by changing the amplification setting during a pedestrian approaching/leaving the  
 211 sensor. It predicts the optimal configuration for the next footstep signal that the sensing  
 212 nodes will detect. To achieve this, the system first detects footstep-induced signals (Step  
 213 Event Detection). Then, it analyzes the detected signals' resolution condition (Signal Res-  
 214 olution Analysis). Finally, based on the analysis, it makes a prediction on the next step's  
 215 amplitude (Optimal Configuration Prediction).

#### 216 5.1.1. Step Event Detection

217 The system detects distinctive signal segments induced by footstep impulses, which we  
 218 refer to as *Step Events* in the rest of the paper. They are extracted from the vibration  
 219 signals through anomaly detection based on a Gaussian model of the background noise (i.e.,  
 220 the signal detected when there is no impulse on the structure) [11]. We utilize a sliding  
 221 window to collect the background noise signal. The system calculates the signal energy for  
 222 each windowed signal, with noise modeled by a Gaussian distribution  $\mathcal{N}(\mu, \sigma)$ . If the signal  
 223 energy in the window falls outside  $3\sigma$  range of the Gaussian model, we consider the window  
 224 to contain a detected step event since it is an abnormal segment.

#### 225 5.1.2. Signal Resolution Analysis

226 Understanding the current Step Event's resolution condition allows the system to predict  
 227 the optimal configuration for the next Step Event. The Step Event resolution is deduced  
 228 from the relation between the analog signal amplitude and resolution shown in Table 2. For  
 229 an N-bit analog-to-digital converter configuration, the  $T_1(v)$  and  $T_2(v)$  are converted to a  
 230 function of  $N$  as  $DT_1(N)$  and  $DT_2(N)$ . These thresholds are applied on the detected Step  
 231 Event range to determine the signal's resolution class based on the relation demonstrated  
 232 in Table 2.

#### 233 5.1.3. Optimal Configuration Prediction

234 The optimal configuration for the next Step Event is obtained using Algorithm shown  
 235 in Figure 4 with two main steps: 1) predict the amplitude of the next Step Event and 2)  
 236 calculate the amplification gain that allows maximum resolution without clipping.

237 To predict the amplitude of the next step signal, the system looks into  $Th_{history}$  number  
 238 of prior step signals' condition. When there are less than  $Th_{history}$  number of steps detected  
 239 in history, the decision is made by prior step signal. If the step history is almost linear,  
 240 which is the most common step energy change behavior when the steps are far away due to

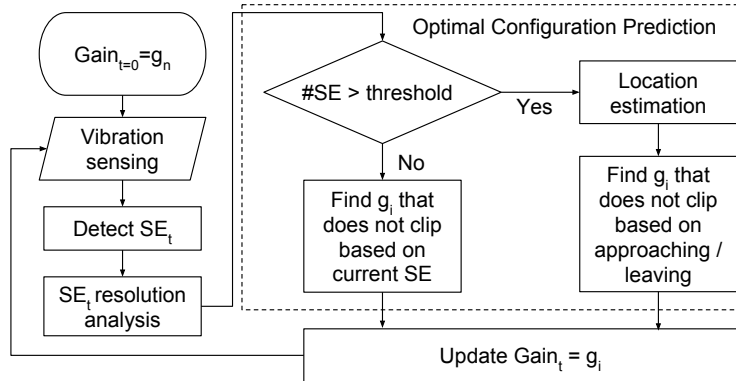


Figure 4: Local profile prediction algorithm.

241 the noise, the system predicts the next step amplitude  $Amp_{t+1}$  with linear model estimated  
 242 from the step history. On the other hand, if the step history is not linear, which occurs  
 243 when steps are near the sensor, the system predicts the next step amplitude  $Amp_{t+1}$  with  
 244 the  $1/d$  model [11] estimated from the step history.

245 To calculate the amplification gain, we separate the cases where the pedestrian ap-  
 246 proaches and leaves the sensing area. When the pedestrian approaches, the system chooses  
 247 to overestimate the predicted amplification by the  $Noise_{Amp}$  in order to find the maximum  
 248 level of amplification gain that will keep  $Amp_{t+1} + Noise_{Amp}$  from getting clipped. On the  
 249 other hand, when the pedestrian leaves, the system chooses to underestimate the predicted  
 250 amplification by the  $Noise_{Amp}$  to find the maximum level of amplification gain that will  
 251 keep  $Amp_{t+1} - Noise_{Amp}$  from getting clipped. Then the system adjusts the amplification  
 252 gain based on this calculation.

## 253 5.2. Global Profile Prediction (GPP)

254 The goal of the GPP is to achieve low distortion (e.g., clipping) for the high amplitude  
 255 step signals by utilizing historical information from neighboring sensors. In practical deploy-  
 256 ments, structural factors such as building beams and partitions, increase footstep strength  
 257 variance. Such complications may cause different sensors to observe different local sensing  
 258 behavior, e.g., if a sensor is deployed near a beam, the detected footstep amplification is  
 259 lower than that of a sensor located between two beams. This type of structural variation  
 260 between different sensors/locations can be propagated through the sensor network based  
 261 on the pedestrian moving direction detection and allow sensors to improve their sensing  
 262 resolution with the historical information from other sensors.

263 GPP can either perform alone or be used with LPP to improve signal fidelity by taking  
 264 structural variation into account. In this section, we introduce how the GPP works alone to  
 265 achieve high resolution signal acquisition for high signal-to-noise ratio step signals. Instead  
 266 of processing on the Step Event level, GPP works on the Trace Event level (the vibration sig-  
 267 nal induced by a person passing by the sensor, containing contiguous detected Step Events).  
 268 First, it obtains the direction of the target trace (Trace Event Direction). Then, it pre-  
 269 dicts the pedestrian's trace (Trace Prediction), i.e., to specific neighbor sensing node, based

270 on walking direction. GPP propagates the pedestrian walking information towards these  
271 neighboring sensing nodes that the pedestrian might pass based on their walking direction.  
272 These nodes rely on their location specifications (Location Specification) and the pedestrian  
273 walking direction to make predictions..

#### 274 *5.2.1. Trace Event Direction Estimation*

275 The Trace Event direction allows our system to determine which neighboring sensing  
276 nodes a pedestrian approaches and which node they are heading away from. So that the  
277 system can inform these neighbor nodes of possible structural anomalies causing signal  
278 changes, which we will detail in Location Specification. At least two sensing nodes are re-  
279 quired to determine the stride direction based on the relative timing of approaching and  
280 leaving different sensors [11]. Each sensing node detects the footstep when a pedestrian  
281 passes by. When the pedestrian approaches then leaves the sensor, their footstep signal  
282 strength will increase then decrease. The spatio temporal information of the footstep signal  
283 with the highest energy within a consecutive footstep sequence detected by different sen-  
284 sors indicates the order in which the pedestrian passes sensors. Therefore the system can  
285 determine which direction (i.e., from/to which sensor) the pedestrian walks.

#### 286 *5.2.2. Trace Prediction*

287 Propagating the information to the neighboring nodes that need it makes the system  
288 robust for ambiguity when people continuously walk by a sensor. To predict which sensor  
289 the pedestrian is walking to, the system models all the deployed nodes as vertexes in a  
290 graph. If there is a physical route that a pedestrian can walk between two vertexes without  
291 passing a third vertex, there is an edge between these two vertexes. We create this graph  
292 heuristically at deployment time as a  $k \times k$  binary table, where  $k$  is the node number, and  
293 the table entry value indicates if there is connectivity between two nodes. We choose the  
294 binary table for computational search efficiency. When a pedestrian walks in the building  
295 and their *stride direction* is detected, the system will notify all the other sensing nodes that  
296 share an edge with this node in the graph except the one that the person walked from.

#### 297 *5.2.3. Location Specification*

298 Due to various structural factors such as beams and partitions, sensors may have different  
299 sensitivity to the same impulse (i.e., same strength and traveling distance). The goal for the  
300 GPP is to achieve high resolution for the high signal-to-noise ratio step signals by utilizing  
301 the historical information from neighboring sensors. When multiple pedestrians walk by  
302 different sensors/locations, the system learns the different impulse response strength between  
303 sensors/locations.

304 When a pedestrian walks by one sensor and is detected, the system models their step  
305 energy change and sends it to the neighboring nodes that the pedestrian will pass by next.  
306 The neighboring node then adjusts its own amplification setting based on the historical data,  
307 which indicates the impulse response strength variation at these different locations. Then  
308 when the pedestrian approaches the neighboring node, the system detects the step signal  
309 with highest energy through the structural variation profile as well as detected step signal  
310 strength from the last sensor.

### 311 5.3. LPP + GPP

312 To achieve high resolution for both low and high amplitude step signals, we combine LPP  
313 and GPP. LPP performs better with low amplitude step signals because the local adjustment  
314 mechanism allows these signals to have higher resolution. However, for high amplitude step  
315 signals, the prediction is highly affected by the variation/noise in the human step strength,  
316 which could lead to over compensation for estimation. On the other hand, GPP performs  
317 better with high amplitude step signals because for those low amplitude step signals within  
318 one trace, there is no adjusting mechanism. However, the fixed amplification means low  
319 amplitude step signals will have low resolution. Therefore, by combining the LPP and the  
320 GPP, the system can achieve better performance in step signal resolution.

321 By combining the LPP and GPP, the system utilizes the LPP to handle step signals with  
322 low amplitude when they are far from the sensor. When the amplitude increases and the  
323 step history is not linear, instead of using the 1/d model as described in Section 5.1.3, the  
324 system relies on the GPP to make the decisions. Instead of using the detected highest step  
325 signal energy, the GPP utilizes the step signal energy changing rate detected by the prior  
326 sensors and matches the current step history changing rate. The system searches the entire  
327 step history of the neighbor nodes and matches the changing rate between continuously  
328 detected  $Th_{history}$  number of steps that has the least square error to that on record. It then  
329 predicts the next step strength.

## 330 6. Implementation

331 To validate our design, we develop a prototype sensing node with  $n = 3$  amplification  
332 settings. We install three operational amplifiers (LMV385) with customized amplification  
333 gains on the sensing configuration board. The processor board is connected to the amplifiers  
334 through three analog-to-digital converter pins. Based on Eq. 10 and the sufficient resolution  
335 range we defined in Section 4, we have  $T_1/T_2 = 1/2$ , which leads to the ratio of the optimal  
336 gains as  $(1/2)^2 : (1/2)^1 : (1/2)^0 = 1 : 2 : 4$ . Through empirical measurements of the other  
337 constants ( $T_1 = 1.5, k = 3 \times 10^{-4}, R = 9$ ) we obtain optimal gains of 2000X, 4000X, and  
338 8000X.

339 The geophone we used is SM-24 [24], with the sensitivity of 28.8V/m/s. The theoretical  
340 sensing range of the sensor is limited by its max coil excursion, which is 2mm. However,  
341 in practical scenarios, the sensing range is limited by the amplifier voltage, which in our  
342 system is 3.3V. Therefore, when an amplifier with  $g_0 = 1$  is applied, the sensing range of  
343 the sensor is 0.1146m/s. When a 10-bits analog-to-digital converter is used, the resolution  
344 of the system is  $1.12 \times 10^{-4}$ m/s, which is not enough to observe signals with peak values  
345 fall in the range of  $10^{-6}$ m/s and  $10^{-4}$ m/s. Therefore, when an amplifier with a gain of  
346 2000X is applied, the sensing range of the sensor is  $5.73 \times 10^{-5}$ m/s, with a resolution of  
347  $5.6 \times 10^{-8}$ m/s. Compare to the setting of  $g_0 = 1$ , this setting has less sensing range but  
348 higher resolution. Similarly, the gain of 4000X and 8000X enables even higher resolution  
349 (respectively  $2.8 \times 10^{-8}$ m/s and  $1.4 \times 10^{-8}$ m/s) with less sensing range (respectively  $2.865 \times$   
350  $10^{-5}$ m/s and  $1.43 \times 10^{-5}$ m/s). Therefore, by combining multiple settings, the system achieves

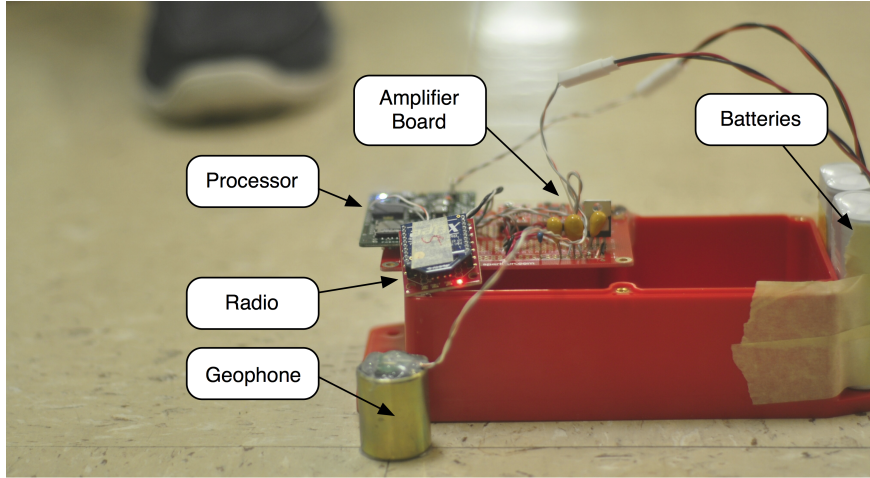


Figure 5: Sensing node.

351 high resolution ( $1.4 \times 10^{-8}$ m/s) as well as high sensing range ( $5.73 \times 10^{-5}$ m/s) at the same  
 352 time.

353 Implemented amplification gains, however, differ slightly due to practical constraints.  
 354 We use two-stage amplifiers in the implementation for better signal filtering, because each  
 355 stage has a differential amplifier serving as a band pass filter. For the first-stage amplifier,  
 356 we selected the resistor value of  $470K\Omega$  over  $10K\Omega$  for the amplification gain  $470/10 = 47$ .  
 357 When selecting the first-stage gain, the corresponding resistor should be available and the  
 358 gain should not cause clipping under most circumstances; otherwise, the clipped signal is  
 359 smoothed by the second-stage's filter. If that happens, the output signal of the second  
 360 stage will not show evidence of clipping, even though it is distorted. For the second-stage  
 361 amplifier, we selected the resistor values of  $470K\Omega$ ,  $1M\Omega$ , and  $2M\Omega$  to achieve the designated  
 362 gain. The calculated gains from this combination were  $2200 \approx 47 \times 47$ ,  $4700 = 47 \times 100$ , and  
 363  $9400 = 47 \times 200$ , respectively. However, due to the limited open loop gain and filtering effects  
 364 of the two-level op-amp circuit, the actual gains of the configuration were approximately  
 365  $g_1 = 2200$ ,  $g_2 = 4400$ , and  $g_3 = 6400$  [25]. With chosen configurations, over 90% of  
 366 the impulses induced by detected footsteps are not clipped with  $g_1$ , and the background  
 367 structural vibration noise after amplification is still less than 1/10 of the entire resolution  
 368 range with  $g_3$ .

369 We placed a prototype sensing node, which is shown in Figure 5, in a hallway and  
 370 collected data from all configurations when a pedestrian passed by, and the signals are shown  
 371 in Figure 6. The blue, red and black lines mark signals collected with configuration of  $g_3$ ,  
 372  $g_2$ , and  $g_1$  respectively. Figures 6 (a, b, and c) are signals collected with fixed configuration,  
 373 from which we can see footstep signals of different amplitude. Figure 6 (d) demonstrates  
 374 the footstep signals of highest resolution without clipping, i.e., the first six footsteps of  
 375  $g_1$  configuration, and the rest signals of  $g_2$  and  $g_3$  configurations. To automatically adapt  
 376 these configurations during sensing, the signal condition prediction is needed, which we will  
 377 explain in the next section.

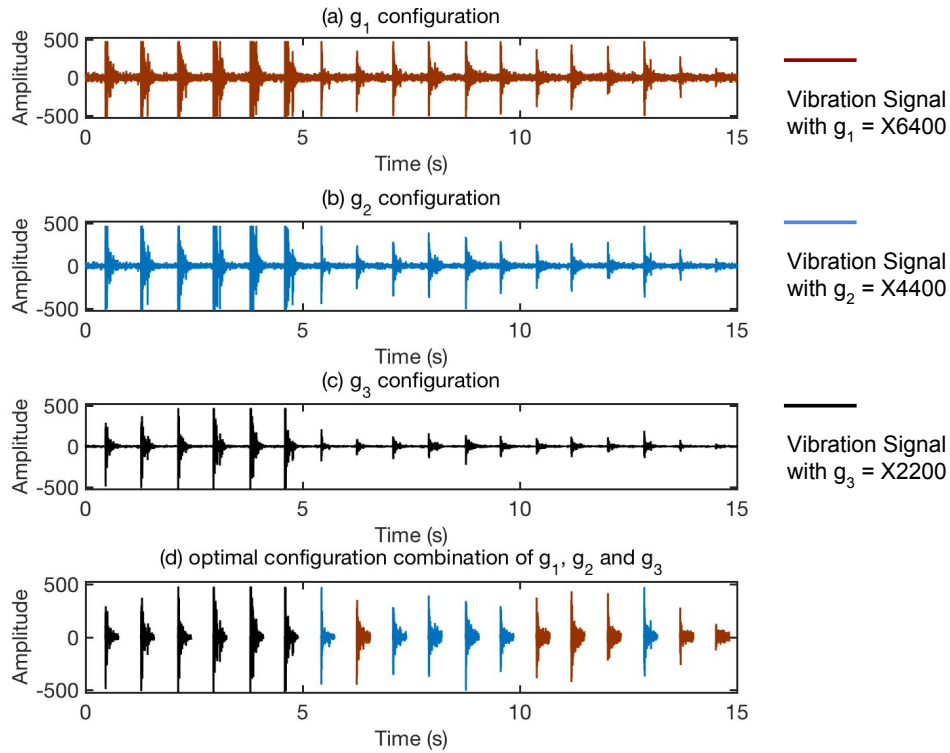


Figure 6: Example of multiple amplification gain configuration. (a, b, and c) are signals collected with amplification gain of 2200, 4400, and 6400. (d) is the signal of optimal resolution selection from events detected in (a, b, and c). The impulses shown as black lines are of gain 2200, and those shown as red lines are of gain 4400. The blue lines are the original line from (a) which is of the starting amplification gain 6400.

## 378 7. Evaluation

379 To understand the system's performance on high fidelity signal acquisition, we conduct  
 380 pedestrian monitoring experiments to evaluate the system. First of all, we introduce the  
 381 metrics used to define the 'high fidelity signal', which is used to measure the performance of  
 382 the system. Next, we present the experiments. Finally, we analyze the results of experiments  
 383 to verify our system design.

### 384 7.1. Evaluation Metrics

385 Signals which exhibit high distortion or low resolution make it difficult if not impossible  
 386 to acquire accurate information on vibrations induced by different impulses. Thus, we define  
 387 'high fidelity signals' to be signals that minimize signal distortion and noise while maximizing  
 388 signal resolution. In this subsection, we present the metrics we use to measure and evaluate  
 389 high fidelity signals quantitatively.



### 390 7.1.1. Signal Resolution

391 Signal resolution in the context of this paper refers to the number of bits used to represent  
392 a signal. We defined the sufficient resolution range in Section 4. To determine if an Step  
393 Event is of sufficient resolution, its *magnitude* is calculated as the maximum absolute value  
394 of the zero mean Step Event signal, and if the magnitude falls into the defined sufficient  
395 resolution range, we consider this Step Event is of sufficient resolution. Therefore, the rate  
396 of Step Events that of sufficient resolution over all the detected Step Events measures the  
397 general signal resolution level. Based on such definition, we define sufficient resolution rate  
398 (SRR) as

$$SRR = \frac{\#sufficient\ resolution\ StepEvents}{\#detected\ StepEvents} \quad (11)$$

399 The higher the SRR value, the more signals of high resolution, and the higher the general  
400 signal resolution. In the analysis, we normalize the SRR by the maximum possible SRR value  
401 the given system hardware configurations can achieve. This normalized SRR evaluates the  
402 performance of LPP and GPP.

### 403 7.1.2. Signal Distortion

404 Signal distortion refers to the degree a measured signal shape differs from the defined  
405 baseline. In this work, we focus on the distortion caused by clipping. Therefore, to measure  
406 the proportion of Step Events that suffers from such distortion, we calculate the clipping  
407 rate of the detected Step Events. The lower the clipping rate, the less signal distortion the  
408 system experiences.

### 409 7.1.3. Signal Magnitude

410 Signal magnitude is defined as the maximum absolute value of a zero-mean step event  
411 signal. It indicates how many digits are actually used to represent the signal. In the ideal  
412 scenario, the system should achieve maximum signal magnitude for each predicted step event  
413 signal. However, due to the variation and randomness in human activities as well as the  
414 monitored structure, the prediction result can vary, i.e., even an Step Event is count as of  
415 sufficient resolution, it might not have maximum magnitude. On the other hand, for different  
416 definitions of sufficient resolution, the same magnitude may be of sufficient or insufficient  
417 resolution. Therefore, we used magnitude to reveal detailed information about each Step  
418 Event.

## 419 7.2. Experiment

420 We conducted experiments to evaluate the system from three different perspectives. First  
421 of all, to understand the variables of the proposed system, we evaluated the calculated con-  
422 figuration setting, LPP, and GPP respectively through a simulation with different numbers  
423 of amplification levels ( $l < n$ ) implemented (Section 7.3). Then to evaluate the signal qual-  
424 ity with the implemented hardware, we placed five sensing nodes in a busy hallway and  
425 measured the signal condition with and without our system (Section 7.4). Finally, we evalu-  
426 ated the system's localization performance by comparing the localization accuracy with and  
427 without the adaptive amplification design (Section 7.5).

428 *7.3. Evaluation I: System Variables*

429 The system design is determined by two factors as discussed in Section 4: 1) the definition  
 430 of sufficient resolution and 2) the implemented number of amplification gains. In this section,  
 431 we specifically evaluate the system behavior in these two factors under perfect amplification  
 432 settings by generating an amplified 10-bit signal through a high resolution oscilloscope signal  
 433 of people walking by one sensor.

434 In total, 15 traces are collected as the seeds for the 10-bit signal generation. Each seed  
 435 generates  $N$  traces of different amplification settings. The minimum amplification gain does  
 436 not have any signal beyond the sufficient resolution, while the maximum amplification gain  
 437 have maximum 0.5% clipped signal among the entire trace of signals. This discrepancy  
 438 means the starting and ending steps are not clipped while most of the close-to-sensor step  
 439 signals are clipped. In total 5 sensors with different structural impulse response strength  
 440 rates are simulated for each collected trace. For the first sensor, the step strength for each  
 441 trace is derived from the seed, and for the rest of the sensors, the step strength for each step  
 442 is calculated with a ratio of  $structural\_rate \times (1 + human\_noise)$  to simulate the human  
 443 behavior noise as well as structural variation.

444 We compare five cases in general: 1) only the LPP algorithm; 2) the baseline, which is  
 445 defined as the median amplification level available; 3) the ground truth, which is the upper  
 446 bound performance the system can achieve with the implemented hardware, i.e., the system  
 447 rejects the settings that result in clipping signal and keeps the highest resolution signal  
 448 that is not clipped; 4) only the GPP algorithm; and 5) both the LPP and GPP conducted  
 449 collaborative sensing as discussed in Section 5.3. The acronyms used in the evaluation  
 450 section are summarized in Table 3.

451 *7.3.1. Sufficient resolution definition*

452 To understand the effects of different sufficient resolution definition, we define the suf-  
 453 ficient resolution parameter as  $T_2 = 1024$  and  $T_1 = i/16 T_2$ , with  $i = 1...15$ . For each  
 454 definition case, we generate  $N$  level of amplified traces as described earlier and run the LPP  
 455 algorithm through the  $N$  level amplifications. Figure 7 demonstrates the SRR, clipping rate,  
 456 and signal magnitude of the results: 1) the blue line with + markers demonstrates the LPP  
 457 algorithm, 2) the red line demonstrates the baseline, 3) the yellow line demonstrates the  
 458 ground truth result, 4) the purple line with circle markers shows the GPP algorithm, and  
 459 5) the green line with cross markers demonstrates results with both LPP and GPP.

460 When the value of  $T_1/T_2$  is low, meaning a large portion of the signal between  $-512$  and  
 461  $512$  is considered as sufficient resolution, the change between different amplification gain

Table 3: Acronyms

Acronym	Meaning
LPP	Local Profile Prediction
GPP	Global Profile Prediction
SRR	Sufficient Resolution Rate

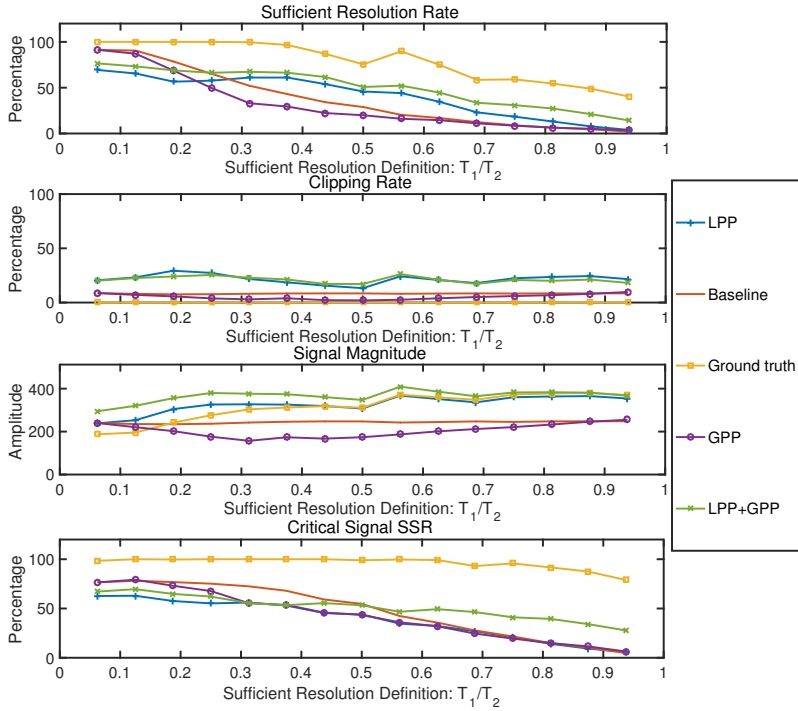


Figure 7: System parameter change: sufficient resolution definition. When the sufficient resolution definition becomes restrict (range  $[T_1, T_2]$  reduces), the SRR reduced for all cases, including LPP, baseline, ground truth, GPP, and LPP+GPP.

462 is large ( $g_{i+1}/g_i = T_2/T_1$ ). Therefore a lower number of amplifiers ( $N$ ) is needed to cover  
463 the variation of the footstep signals. This also means that more low magnitude step signals  
464 are considered sufficient resolution, and have a high SRR value and low signal magnitude  
465 value. With the increase of the value of  $T_1/T_2$ , the clipping rate remains stable, while the  
466 signal magnitude increases. This means that the signal quality increases, but due to the  
467 increment of the sufficient resolution definition, the SRR decreases. In addition, since the  
468 GPP is focused on decreasing the clipping rate and hence increasing the sufficient resolution  
469 rate, we further explore a fourth metric, the critical signal SSR, which includes only 5 steps  
470 with the highest signal-to-noise ratio in a trace.

471 LPP in general outperforms the baseline when the definition of the sufficient resolution is  
472 over 1/4 of the entire resolution range in terms of SRR and signal magnitude by an average  
473 of 5% and 34% respectively. GPP reduces the clipping rate when compared to the baseline  
474 when the sufficient resolution is between 1/4 and 3/4 of the entire resolution range, therefore  
475 causing a clipping rate 1.6X lower and lowering the signal magnitude as well. When LPP  
476 and GPP are combined, the SRR is higher than either algorithm performing alone by 10% on  
477 average and raises the signal magnitude by 12% on average. In general, for all the metrics,  
478 the LPP and GPP combination follows the trend of LPP and outperforms the LPP most  
479 in the critical step signals with high signal-to-noise ratio. This advantage shows an average  
480 increase of 10% and up to 4X increase for the highest  $T_1/T_2$  value when the definition of the

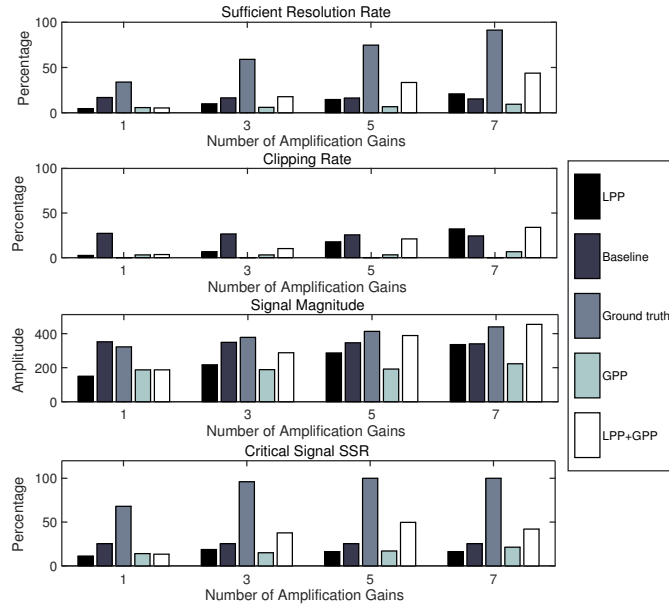


Figure 8: System parameter change: number of amplification gains. When the number of amplification gain implemented is increased, the SRR of the ground truth and the LPP+GPP increases. The clipping rate of the ground truth remains zero since the system can always reject the clipped signal, while that of the LPP+GPP increase due to the prediction error.

481 sufficient resolution is of a high standard ( $T_1/T_2$  value high) for the critical step signal SRR.

### 482 7.3.2. Number of amplifications

483 In an ideal scenario, the system could have an infinite number of amplification levels to  
 484 cover an infinite range of amplification needs. However, in reality, only a limited number of  
 485 amplification levels can be implemented. Because of this, the number of amplifications actu-  
 486 ally implemented affects the amplification range the system can achieve and therefore affects  
 487 the system performance. Based on the results from the experiment results in Section 7.3.1,  
 488 we selected the definition of  $T_1/T_2 = 12/16$ , which introduces seven levels of amplification  
 489 gains. The number is selected so that there are large enough available amplification gains  
 490 involved to demonstrate the system performance when different numbers of amplification  
 491 gains are implemented.

492 To understand the number of implementation of amplifications, we selected the median  
 493 level of amplification, then increase the number of levels by adding one smaller and one  
 494 larger amplification gain each time, and explore the system performance with these different  
 495 number of gains. Figure 8 shows the evaluation results of SRR, clipping rate and the  
 496 signal magnitude when these different numbers of amplification gains are used. Each metric  
 497 shows an increase trend for all evaluated scenarios except baseline, since baseline is a fixed  
 498 amplification setting only affected by the definition of the sufficient resolution rate. The  
 499 more amplification gain levels are implemented, the more adaptable levels can be used for  
 500 selection, therefore increasing the sufficient resolution rate and signal magnitude. On the

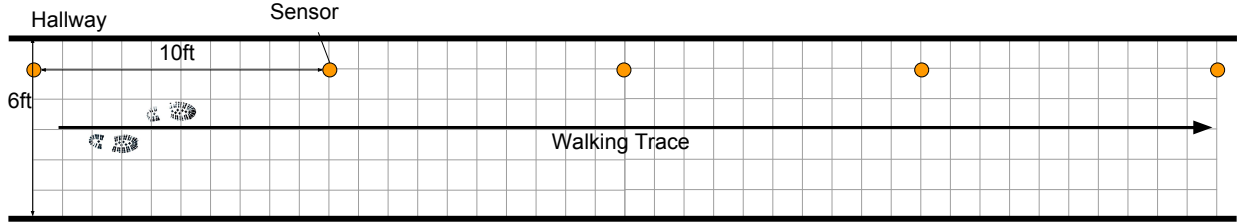


Figure 9: Deployment floor-plan of experimental setups in a school building. Five sensing nodes are deployed in a straight line, approximately three meters apart. Sensors are directly attached to the floor.

501 other hand, the more choices on the high amplification gains the system is allowed to have,  
 502 the higher chance the system may select a high amplification gain that causes clipping, hence  
 503 the increasing clipping rate as well.

#### 504 7.4. Evaluation II: Adaptive Amplification

505 To evaluate the system performance in the real-world scenario, we conducted the exper-  
 506 iment with a small-scale deployment of five sensing nodes in a school building. We mounted  
 507 these sensing nodes in a hallway (approximately  $20m \times 2m$  area, tile floor) inside the school  
 508 building as shown in Figure 9. The system sampled the vibration data at 1000 Hz in three  
 509 amplification configurations. The Real-Time-Clock module on each sensing node provided  
 510 timestamps for each sensing node’s data collection. 10 subjects were asked to walk natu-  
 511 rally down a hallway with no restriction on activities (e.g. cell phones, conversing), with the

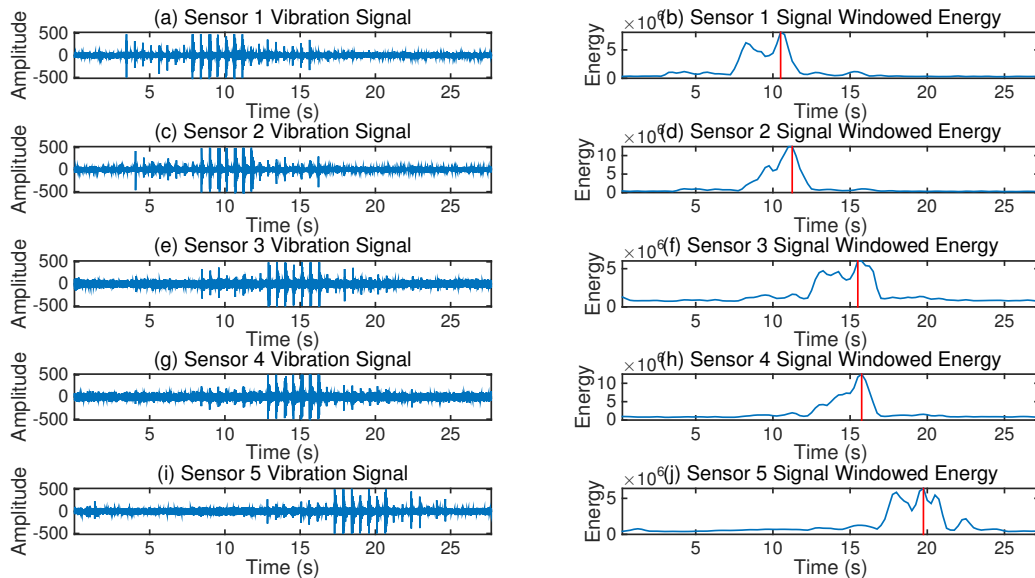


Figure 10: Structural vibration signal detected by sensors when a pedestrian walks by.

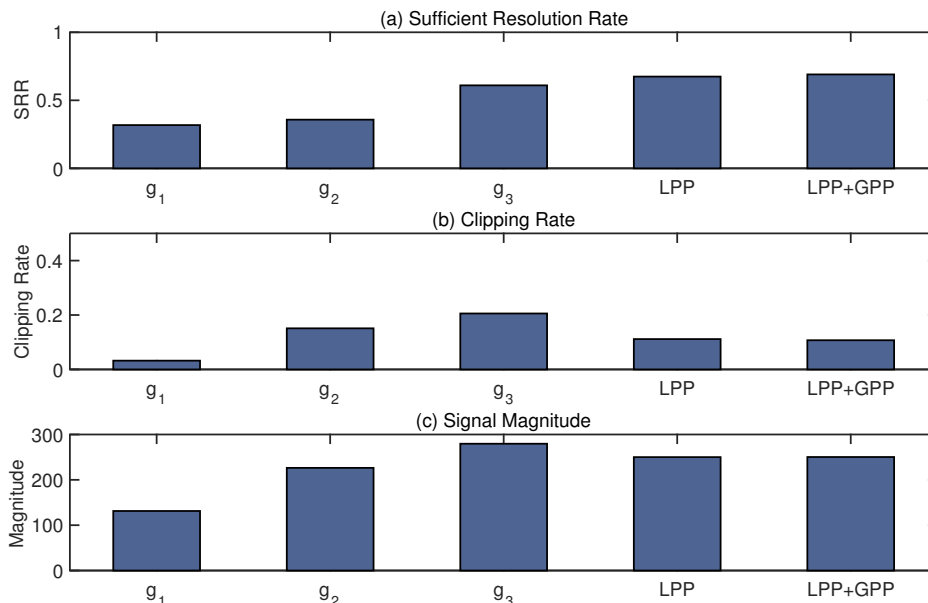


Figure 11: Evaluation of the system with the system performance experiment. Approximate amplification ratios for fixed sensing configurations are  $g_1 = 2200$ ,  $g_2 = 4400$ , and  $g_3 = 6400$ . The performance of LPP, as well as LPP+GPP has higher SRR than the fixed configurations.  $g_3$  has highest average signal magnitude resulting from its high clipping rate. Therefore, LPP+GPP’s over all performance is improved compared to fixed amplification gains. GPP results are similar to LPP results due to the lack of structural effects in this experiment.

512 footstep data being picked up by the system. Figure 10 demonstrates an example of one of  
 513 the subjects walks along the hallway passing five sensors deployed.

514 With the data from the experiment, we conduct configuration adaptation to compare  
 515 our system (LPP + GPP) with fixed configurations. Figure 11 (a) shows the normalized  
 516 SRR from three different fixed amplification configurations ( $g_1 = 2200$ ,  $g_2 = 4400$ , and  
 517  $g_3 = 6400$ ), an adaptive configuration using only LPP, and an adaptive configuration with  
 518 LPP+GPP respectively 32%, 36%, 61%, 67%, and 69%. The system improvement compar-  
 519 ing to  $g_1$ ,  $g_2$ , and  $g_3$  are at least 1.7X and up to 2X. Note that the algorithm is designed for  
 520 regular footsteps, i.e., footsteps from the same person are assumed to be same impulses, and  
 521 uses fixed padding values ( $P_1$  and  $P_2$  as described in Section 5.1.3). However, the random-  
 522 ness in human footsteps introduced prediction errors, leading to an approximately 30% lower  
 523 SRR value compared to hardware limitation. The LPP achieves higher SRR compared to  
 524 that of  $g_1$ ,  $g_2$ , and  $g_3$ .  $g_3$  and  $g_2$  amplify the near field signal so that many of the signals are  
 525 clipped, leading to low count on sufficient resolution rate. To validate that, we also demon-  
 526 strated clipping rate of these configurations in Figure 11 (b), of which values are respectively  
 527 3%, 15%, 21%, 11%, and 11%.  $g_1$  obtains most of the near field signals without clipping, but  
 528 the far field signals are of low resolution due to insufficient amplification, therefore lowering  
 529 the SRR. In order to understand the low resolution effects, we also present average signal

530 magnitude in Figure 11 (c). As mentioned earlier, the magnitude of a signal is defined as  
531 the maximum absolute value of the zero mean signal. The figure shows that fixed gains have  
532 an expected effect on magnitude while LPP and GPP sometimes reduce and increase gain  
533 as needed. The GPP only made slightly higher SRR comparing to LPP in this experiment  
534 due to the relative uniform nature of the structure.

### 535 *7.5. Evaluation III: Application*

536 We further investigated the system with the application of 1-D localization based on  
537 a footstep induced vibration amplitude decay model [26]. Based on the Rayleigh wave  
538 propagation model, we used the system to locate where the pedestrian passes the sensor  
539 in a hallway. Accurately detecting the passing point allows localization of the person in  
540 one dimension. To evaluate that, we fixed the parameters we investigated in Section 7.3 to  
541  $T_1/T_2 = 12/16$  and the number of amplification levels as 7. Then we selected the detected  
542 step signal with the highest amplitude as the passing point. We compared the step count  
543 error of our system to that of the fixed amplification, in this case selecting the middle level  
544 (level 4). The average error for our system in detecting the step where the pedestrian is  
545 passing the sensor is 0.47m, and the average error for the fixed amplification is 1.13m. Our  
546 system shows a 2X less step error when used to locate the pedestrian steps.

## 547 **8. Discussion**

548 In this section, we discuss the system limitations, the design trade off, the multiple  
549 pedestrian sensing condition, and the motivating use-cases for the system.

### 550 *8.1. System Limitations*

551 The limitations of our system come from mainly two assumptions: 1) the assumption that  
552 pedestrian induced structural vibrations have the signal-strength that can be predicted, and  
553 2) the assumption that the algorithm selects from the amplification configurations so that the  
554 monitored signal has a sufficient resolution using at least one of the amplifier gains. When  
555 the pedestrian induced structural vibration strength is not predictable, e.g., erratic crowd  
556 behavior, the system prediction accuracy will decrease, which will reduce the signal fidelity.  
557 When the monitored signal is extremely high or low in amplitude, the system configuration  
558 may always be clipping or of insufficient resolution, despite the accurate prediction, due to  
559 limited number of amplifier configurations.

### 560 *8.2. Design Trade-offs*

561 Our system implementation considers the trade-offs between a number of analog-to-  
562 digital converters and the sampling rate. When the system has access to a large enough  
563 number of analog-to-digital converters, which connects to a large enough number of ampli-  
564 fication settings, and can sample at a high enough rate, the system, in theory, can obtain  
565 highest resolution signal for all monitored structural responses. When the number of analog-  
566 to-digital converters is limited, and the sampling rate is high enough, the system can still  
567 obtain signals from all available amplification settings. In this case, the system can reject

568 clipped signals, and keep the highest resolution signal without clipping, which is the ground  
569 truth scenario in our evaluation. In many practical scenarios, however, it is difficult if not  
570 impossible for the system to sample many analog-to-digital converters at the same time,  
571 due to limited sampling rates. Then the LPP and GPP are used to predict and select the  
572 amplification settings needed, and the prediction errors cause the clipping and insufficient  
573 resolution incidences we see in the evaluation.

### 574 *8.3. Multiple People Sensing*

575 When multiple people passing the sensing area at the same time, the vibration signals  
576 induced by their steps mix. When people passing by the sensing area in a different manner  
577 (side by side, one after another, towards each other, etc.), their footstep signals may show  
578 different energy change patterns, which may not agree with the heuristic rules used in LPP.  
579 In this case, our system can utilize the mobility model of the pedestrians and rely on the  
580 GPP more than LPP to achieve more stable prediction of the structural response strengths.

### 581 *8.4. Motivating Use-cases*

582 Monitoring human activity induced excitations enables human information inference.  
583 When people walk on the floor, the footstep induced structural vibration can be used to  
584 tracking, identify, and count pedestrian in the sensing area [11, 9, 3, 13]. When people  
585 lie on the bed, their heartbeats induced vibration can also be detected, hence be used  
586 for health status estimation [27]. When people cook in the kitchen, play games in the  
587 living room, or cleaning in the house, their interaction with the physical environment induce  
588 structural vibration too, which enables activity recognition [28]. Furthermore, this inevitable  
589 interaction with the objects in the physical environment makes it possible to turn ambient  
590 objects with a flat solid surface into a touch screen [14]. These types of information enable  
591 smart home applications such as kid monitoring, kitchen safety monitoring. When deployed  
592 in large-scaled scenarios, such as in a nursing home or hospital, the human activity induced  
593 excitation monitoring can enable patient/elderly monitoring.

## 594 **9. Conclusion**

595 In this paper, we introduce a high fidelity structural vibration acquisition sensing sys-  
596 tem. It is an easy-to-install sparse sensing system that improves the sensing signal fidelity  
597 through adapting hardware configurations based on target signal prediction. The prediction  
598 is achieved through two key aspects: 1) each individual sensor predict the step strength  
599 change based on a pedestrian walking model, 2) networked devices collaboratively predict  
600 the step strength through a global profile on a structural variation model. In our pedestrian  
601 footstep monitoring application, our system demonstrated up to 2X increase on SRR in our  
602 evaluation experiments and up to 2X less error rate when used to locate the pedestrian when  
603 they walk along the hallway. We believe that such a signal acquisition system can be ap-  
604 plied to various future applications in smart buildings for human activity induced excitation  
605 vibration data acquisition.



606 **Acknowledgements**

607 This work is partially supported by Intel, Pennsylvania Infrastructure Technology Al-  
608 liance (PITA), CMU-SYSU Collaborative Innovation Research Center (CIRC), and Google.

609 **References**

- 610 [1] A. Ekimov, J. M. Sabatier, Vibration and sound signatures of human footsteps in buildings), The  
611 Journal of the Acoustical Society of America 120 (2) (2006) 762–768.
- 612 [2] A. Itai, H. Yasukawa, Footstep classification using simple speech recognition technique, in: Circuits  
613 and Systems, 2008. ISCAS 2008. IEEE International Symposium on, IEEE, 2008, pp. 3234–3237.
- 614 [3] S. Pan, N. Wang, Y. Qian, I. Velibeyoglu, H. Y. Noh, P. Zhang, Indoor person identification through  
615 footstep induced structural vibration, in: Proceedings of the 16th International Workshop on Mobile  
616 Computing Systems and Applications, ACM, 2015, pp. 81–86.
- 617 [4] D. Bales, P. Tarazaga, M. Kasarda, D. Batra, Gender classification using under floor vibration mea-  
618 surements, in: Dynamics of Coupled Structures, Volume 4, Springer, 2016, pp. 377–383.
- 619 [5] D. Bales, P. Tarazaga, M. Kasarda, D. Batra, A. Woolard, J. D. Poston, V. Malladi, Gender classifi-  
620 cation of walkers via underfloor accelerometer measurements, IEEE Internet of Things Journal (2016)  
621 1259 – 1266.
- 622 [6] M. Mirshekari, S. Pan, A. Bannis, Y. P. M. Lam, P. Zhang, H. Y. Noh, Step-level person localization  
623 through sparse sensing of structural vibration, in: Proceedings of the 14th International Conference on  
624 Information Processing in Sensor Networks, ACM, 2015, pp. 376–377.
- 625 [7] J. D. Poston, J. Schloemann, R. M. Buehrer, V. Malladi, A. G. Woolard, P. A. Tarazaga, Towards  
626 indoor localization of pedestrians via smart building vibration sensing, in: Localization and GNSS  
627 (ICL-GNSS), 2015 International Conference on, IEEE, 2015, pp. 1–6.
- 628 [8] J. Schloemann, V. S. Malladi, A. G. Woolard, J. M. Hamilton, R. M. Buehrer, P. A. Tarazaga, Vibration  
629 event localization in an instrumented building, in: Experimental Techniques, Rotating Machinery, and  
630 Acoustics, Volume 8, Springer, 2015, pp. 265–271.
- 631 [9] M. Mirshekari, S. Pan, P. Zhang, H. Y. Noh, Characterizing wave propagation to improve indoor  
632 step-level person localization using floor vibration, in: SPIE Smart Structures and Materials+ Nonde-  
633 structive Evaluation and Health Monitoring, International Society for Optics and Photonics, 2016, pp.  
634 980305–980305.
- 635 [10] K. Dobbler, M. Fišer, M. Fellner, B. Rettenbacher, Vibroacoustic monitoring: Techniques for human  
636 gait analysis in smart homes, in: Ambient Assisted Living, Springer, 2014, pp. 47–58.
- 637 [11] S. Pan, A. Bonde, J. Jing, L. Zhang, P. Zhang, H. Noh, Boes: building occupancy estimation system  
638 using sparse ambient vibration monitoring, in: SPIE Smart Structures and Materials+ Nondestructive  
639 Evaluation and Health Monitoring, International Society for Optics and Photonics, 2014, pp. 90611O–  
640 90611O–16.
- 641 [12] A. Subramanian, K. G. Mehrotra, C. K. Mohan, P. K. Varshney, T. Damarla, Feature selection and  
642 occupancy classification using seismic sensors, in: International Conference on Industrial, Engineering  
643 and Other Applications of Applied Intelligent Systems, Springer, 2010, pp. 605–614.
- 644 [13] S. Pan, M. Mirshekari, P. Zhang, H. Y. Noh, Occupant traffic estimation through structural vibration  
645 sensing, in: SPIE Smart Structures and Materials+ Nondestructive Evaluation and Health Monitoring,  
646 International Society for Optics and Photonics, 2016, pp. 980306–980306.
- 647 [14] S. Pan, C. Ramirez, M. Mirshekari, J. Fagert, A. J. Chung, C. C. Hu, J. P. Shen, H. Y. Noh, P. Zhang,  
648 Surfacevibe: Vibration-based tap & swipe tracking on ubiquitous surfaces, in: Information Processing  
649 in Sensor Networks (IPSN), 2017 15th ACM/IEEE International Conference on, IEEE, 2017, pp. 1–12.
- 650 [15] A. Barzilai, Improving a geophone to produce an affordable broadband seisometer, Mechanical Engi-  
651 neering, Stanford University Jan. 25.

- 652 [16] A. Janssen, R. Veldhuis, L. Vries, Adaptive interpolation of discrete-time signals that can be modeled  
653 as autoregressive processes, *Acoustics, Speech and Signal Processing*, IEEE Transactions on 34 (2)  
654 (1986) 317–330.
- 655 [17] S. Kitic, L. Jacques, N. Madhu, M. P. Hopwood, A. Spriet, C. De Vleeschouwer, Consistent iterative  
656 hard thresholding for signal declipping, in: *Acoustics, Speech and Signal Processing (ICASSP)*, 2013  
657 IEEE International Conference on, IEEE, 2013, pp. 5939–5943.
- 658 [18] S. Miura, H. Nakajima, S. Miyabe, S. Makino, T. Yamada, K. Nakadai, Restoration of clipped audio  
659 signal using recursive vector projection, in: *TENCON 2011-2011 IEEE Region 10 Conference*, IEEE,  
660 2011, pp. 394–397.
- 661 [19] W. Loetwassana, R. Puchalard, A. Lorsawatsiri, J. Koseeyaporn, P. Wardkein, Adaptive howling  
662 suppressor in an audio amplifier system, in: *2007 Asia-Pacific Conference on Communications*, IEEE,  
663 2007, pp. 445–448.
- 664 [20] J. Zhang, R. Wang, S. Lu, J. Gong, Z. Zhao, H. Chen, L. Cui, N. Wang, Y. Yu, Easicprs: design  
665 and implementation of a portable chinese pulse-wave retrieval system, in: *Proceedings of the 9th ACM*  
666 *Conference on Embedded Networked Sensor Systems*, ACM, 2011, pp. 149–161.
- 667 [21] A. C. Krochmal, D. P. Stewart, J. E. Whitecar, Variable distortion limiter using clip detect predictor,  
668 uS Patent 7,202,731 (Apr. 10 2007).
- 669 [22] T. G. Gutowski, C. L. Dym, Propagation of ground vibration: a review, *Journal of Sound and Vibration*  
670 49 (2) (1976) 179–193.
- 671 [23] H. Verhas, Prediction of the propagation of train-induced ground vibration, *Journal of Sound and*  
672 *Vibration* 66 (3) (1979) 371–376.
- 673 [24] Geophone sm-24, <https://www.sparkfun.com/products/11744>, accessed: 2017-01-24 (2006).
- 674 [25] R.-t.-R. Low-Voltage, LMV321, LMV358, LMV324 (2009).
- 675 [26] I. A. Viktorov, Rayleigh and Lamb waves: physical theory and applications, Plenum press, 1970.
- 676 [27] Z. Jia, M. Alaziz, X. Chi, R. E. Howard, Y. Zhang, P. Zhang, W. Trappe, A. Sivasubramaniam, N. An,  
677 Hb-phone: a bed-mounted geophone-based heartbeat monitoring system, in: *Information Processing in*  
678 *Sensor Networks (IPSN)*, 2016 15th ACM/IEEE International Conference on, IEEE, Vienna, Austria,  
679 2016, pp. 1–12.
- 680 [28] P. A. Kodeswaran, R. Kokku, S. Sen, M. Srivatsa, Idea: A system for efficient failure management  
681 in smart iot environments, in: *Proceedings of the 14th Annual International Conference on Mobile*  
682 *Systems, Applications, and Services*, ACM, 2016, pp. 43–56.